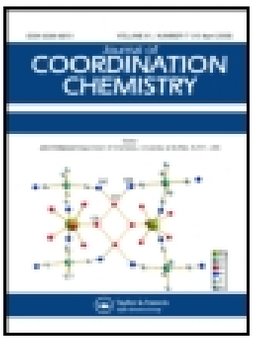

Journal of Coordination Chemistry

ISSN: 0095-8972 (Print) 1029-0389 (Online) Journal homepage: http://www.tandfonline.com/loi/gcoo20

Three lanthanide complexes with mixed salicylate and 1,10-phenanthroline: Syntheses, crystal structures and luminescent/magnetic properties

Min Hu, Ling-Yu Yue, E. Carolina Sañudo & Shao-Ming Fang

To cite this article: Min Hu, Ling-Yu Yue, E. Carolina Sañudo & Shao-Ming Fang (2016): Three lanthanide complexes with mixed salicylate and 1,10-phenanthroline: Syntheses, crystal structures and luminescent/magnetic properties, Journal of Coordination Chemistry, DOI: 10.1080/00958972.2016.1198477

To link to this article: http://dx.doi.org/10.1080/00958972.2016.1198477

Publisher: Taylor & Francis
Journal: *Journal of Coordination Chemistry*
DOI: http://dx.doi.org/10.1080/00958972.2016.1198477

Three lanthanide complexes with mixed salicylate and 1,10-phenanthroline: Syntheses, crystal structures and luminescent/magnetic properties

MIN HU*†, LING-YU YUE†, E. CAROLINA SAÑUDO‡ and SHAO-MING FANG†

†Zhengzhou University of Light Industry, Henan Provincial Key Laboratory of Surface & Interface Science, Zhengzhou, Henan 450000, P. R. China
‡Departament de Química Inorgànica i Institut de Nanociència i Nanotecnologia, Universitat de Barcelona, Diagonal 645, 08028 Barcelona Spain

Three new lanthanide complexes incorporating salicylate (**HSA** or **SA**) and 1,10-phenanthroline (phen), $Ln_3(HSA)_5(SA)_2(phen)_3$ [Ln = Ho (**1**) and Er (**2**)] and $Sm_2(HSA)_2(SA)_2(phen)_3$ (**3**), have been synthesized. X-ray structural analysis reveals that **1** and **2** are isostructural with a trinuclear pattern and **3** exhibits a binuclear structure. Comparison of the structural differences between **1/2** and **3** suggests that the identity of metal plays an important role in construction of such complexes. The magnetic properties of **1** are discussed. Moreover, **2** and **3** are both photoluminescent materials, and their emission properties are closely related to their corresponding Ln^{III} centers.

Keywords: Lanthanide complexes; Salicylate linker; Crystal structure; Magnetic/luminescence properties

1. Introduction

Syntheses of lanthanide carboxylate materials attract attention due to their desirable structures [1] and potential applications arising from luminescence [2] and magnetic properties [3]. Organic ligands play a vital role in tuning the structural topology and functionality of such compounds [4]. The use of aromatic ligands is common as they are excellent in sensitizing the lanthanide luminescence by the well-known "antenna effect" [5]. A number of aromatic carboxylate ligands

*Corresponding author. Email: humin@zzuli.edu.cn

such as benzoate and modified benzoates are known [6]; salicylic acid (H_2**SA**), a type of aromatic carboxylate ligand with one carboxyl and one hydroxyl arranged in a 1,2-fashion around the central aromatic group, can form various coordination structures [7]. Carboxylate and hydroxy groups on the molecules can be partially or completely deprotonated to form versatile coordination models; the hydroxyl group may provide an additional binding site to generate more complicated structures in cooperation with the carboxyl groups. Furthermore, the phenyl can form C/O–H···O, C/O–H···π and π···π interactions as steering forces in the control of molecular self-assembly. Chelating ligands such as 1,10-phenanthroline (phen) may inhibit expansion of the polymeric framework to give coordination polymers of low-dimensionality or zero-dimensional molecules [8].

Keeping these observations in mind, we have reported isomorphous Dy^{III} and Gd^{III} complexes with H_2**SA** and phen as ligands, in which a luminescent linear trinuclear Dy^{III} complex exhibits slow magnetic relaxation of single ion origin [7d]. These results indicate that H_2**SA** is an excellent ligand in the self-assembly of coordination complexes and further efforts are required to provide more information on its coordination behavior. As an extension of the above work, three new lanthanide complexes, Ln_3(H**SA**)$_5$(**SA**)$_2$(phen)$_3$ [Ln = Ho (**1**) and Er (**2**)] and Sm_2(H**SA**)$_2$(**SA**)$_2$(phen)$_3$ (**3**), based on H**SA/SA** and phen ligands were obtained. Herein, we report the syntheses, crystal structures, and luminescent properties of these complexes.

2. Experimental

2.1. *Materials and general methods*

All the starting reagents and solvents for synthesis were commercially available and used as received. Elemental analyses (C, H and N) were performed on a Vario EL III Elementar analyzer. IR spectra were recorded from 4000–400 cm^{-1} on a Tensor 27 OPUS (Bruker) FT-IR spectrometer with KBr pellets. Thermogravimetric analysis (TGA) experiments were carried out on a Perkin-Elmer Diamond SII thermal analyzer from room temperature to 800 °C under nitrogen at a heating rate of 10 °C min^{-1}. The emission spectra in the visible region were tested on a F-7000 (HITACHI) spectrophotometer and those in near-infrared region were measured on an FLS-980 fluorescence spectrophotometer.

2.2. *Synthesis of 1-3*

All three complexes were prepared with similar methods. A general synthetic procedure is described as follows by using **1** as an example.

2.2.1. $Ho_3(HSA)_5(SA)_2(phen)_3$ (1). A mixture of Ho_2O_3 (0.2 mmol, 0.076 g), H_2**SA** (1.5 mmol, 0.207 g), phen (0.4 mmol, 0.079 g) and H_2O (15 mL) was placed in a Teflon-lined stainless steel vessel (23 mL), heated to 140 °C for 72 h, and then cooled to room temperature at a rate of 5 °C h^{-1}. Single crystals of **1**-**3** suitable for X-ray diffraction were obtained. Then the obtained crystals were collected by filtration, washed with water and ethanol, and dried in air. Yield: 0.25 g (60% based on H_2**SA**). Elemental Anal. Calc. for $C_{85}H_{57}Ho_3N_6O_{21}$: C, 51.22; H, 2.88; N, 4.22. Found: C, 51.31; H, 2.75; N, 4.39%. The IR spectrum for **1** is shown in figure S1a.

2.2.2. $Er_3(HSA)_5(SA)_2(phen)_3$ (2). The same synthetic method as that for **1** was used except that Ho_2O_3 was replaced by Er_2O_3 (0.2 mmol, 0.077 g). Yield: 0.24 g (55% based on H_2**SA**). Elemental Anal. Calc. for $C_{85}H_{57}Er_3N_6O_{21}$: C, 51.04; H, 2.87; N, 4.20. Found: C, 51.33; H, 2.95; N, 4.31%. The IR spectrum for **2** is shown in figure S1b.

2.2.3. $Sm_2(HSA)_2(SA)_2(phen)_3$ (3). The same synthetic method as that for **1** was used except that Ho_2O_3 was replaced by Sm_2O_3 (0.2 mmol, 0.070 g). Yield: 0.31 g (60% based on H_2**SA**). Elemental Anal. Calc. for $C_{32}H_{19}N_4O_5Pr$: C, 55.39; H, 3.05; N, 6.06. Found: C, 55.21; H, 3.28; N, 6.29%. The IR spectrum for **3** is shown in figure S1c.

2.3. *Crystal structure determinations of 1-3*

X-ray single-crystal diffraction data for **1**-**3** were collected on an Xcalibur Gemini Eos CCD diffractometer at 294(2) K with Mo-*K*α radiation (λ = 0.71073 Å) by ω scan mode. The program SAINT [9] was used for integration of the diffraction profiles. Semi-empirical absorption corrections were applied using SADABS [10]. All the structures were solved by direct methods using the SHELXS program of the SHELXTL package and refined by full-matrix least-squares methods with SHELXL [11]. Metal ions in each complex were located from the *E*-maps and other non-hydrogen atoms were located in successive difference Fourier syntheses and refined with anisotropic thermal parameters on F^2. Hydrogens were geometrically positioned and refined

using a riding model. Further crystallographic data and structural refinement details for **1**-**3** are summarized in table 1. Selected bond lengths and angles are listed in tables S1-S3. CCDC Nos. 1446491–1446493 contain the supplementary crystallographic data for **1**-**3**, respectively. These materials can be obtained free of charge via http://www.ccdc.cam.ac.uk/conts/retrieving.html, or from the Cambridge Crystallographic Data Centre, 12 Union Road, Cambridge CB2 1EZ, UK; Fax: (+44) 1223-336-033; or E-mail: deposit@ccdc.cam.ac.uk.

2.4. *Magnetic measurements*

Magnetic measurement for **1** was carried out in the Unitat de Mesures Magnètiques (Universitat de Barcelona) on polycrystalline samples (*circa* 30 mg) with a Quantum Design SQUID MPMS-XL magnetometer equipped with a 5 T magnet. Diamagnetic corrections were calculated using Pascal's constants and an experimental correction for the sample holder was applied.

3. Results and discussion

3.1. *Descriptions of crystal structures*

3.1.1. $Ho_3(HSA)_5(SA)_2(phen)_3$ (1) and $Er_3(HSA)_5(SA)_2(phen)_3$ (2). Single-crystal X-ray structure analyses revealed that **1** and **2** are isostructural (figures 1 and S4); therefore, **1** is taken as an example to discuss in detail. Complex **1** crystallized in the monoclinic system with a $P2_1/c$ space group. The asymmetric unit consists of three crystallographically unique Ho^{III} ions, five H**SA** ligands, two **SA** ligands and three phen ligands. Three Ho^{III} centers adopt a nearly linear arrangement (figure 1) as confirmed by the Ho1–Ho3–Ho2 angle of 165.29(5)° and are all eight-coordinate, but surrounded by different donors (figure S2 and table S1). Ho1 is coordinated to six oxygens (O1, O4, O5, O7, O11 and O12) from four H**SA/SA** ligands and two nitrogens (N1 and N2) from one phen. For Ho2, the polyhedron is defined by four oxygens (O13, O17, O18 and O19) from three distinct H**SA/SA** ligands and four nitrogens (N3, N4, N5 and N6) from two phen ligands. Ho3 is coordinated to eight oxygens (O2, O8, O10, O11, O14, O16, O17 and O20) from six distinct H**SA/SA** ligands. Though all three ions show coordination geometries of a distorted triangular dodecahedron, they are slightly different. Ho3 is in a distorted triangular dodecahedron, while Ho1 and Ho2 are in different distorted bicapped trigonal prism geometries (figure S2). All bond lengths around the metal are comparable to those found in other reported Ho^{III} complexes [12]. In the structure of **1**, there are three types of coordination modes for the

H**SA/SA** ligands: a μ_2-μ^1:μ^1 double monodentate bridging mode (scheme 1A), a μ_1-μ^1:μ^1 bidentate chelating mode (scheme 1B) and a μ_2-μ^1:μ^2 bridging mode linking two lanthanide ions (scheme 1C). Adjacent Ho ions are linked via the μ_2-bridging carboxylate groups of H**SA/SA** to generate trinuclear building units. The structure of **1** contains numerous C–H···O hydrogen bonds and C–H···π supramolecular interactions (table S4), which link such Ho_3 motifs into a 1D (figure 1b), 2D (figure S3) and further an overall 3D supramolecular framework (figure 1c).

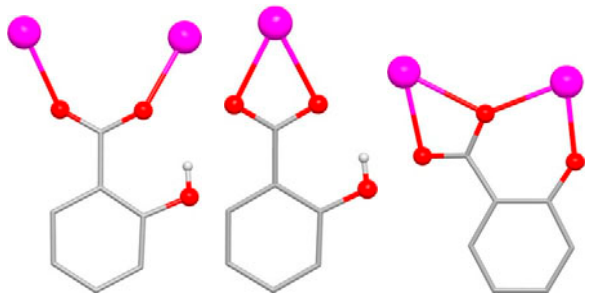

A B C

Scheme 1. Coordination modes of H**SA/SA** in **1**-**3**.

3.1.2. $Sm_2(HSA)_2(SA)_2(phen)_3$. X-ray diffraction analysis revealed that the asymmetric unit of **3** consists of two crystallographically unique Sm ions, two H**SA** ligands and two **SA** ligands. The coordination environment of the central Sm^{III} is shown in figure 2a with atom numbering. The two Sm^{III} ions are nine-coordinate but surrounded by different donors (figure S5). Sm1 is coordinated by five oxygens (O1, O3, O4, O5 and O7) from three H**SA/AS** ligands and four nitrogens (N1, N2, N3 and N4) from two phen ligands to form a distorted tricapped trigonal prism geometry. Sm2 has seven oxygens (O1, O2, O4, O6, O8, O10 and O11) from four H**SA/AS** ligands and two nitrogens (N5 and N6) from one phen to form a distorted monocapped square antiprism (figure S5). All Sm–O and Sm–N bond lengths are comparable to those reported earlier for Sm complexes [13]. In the structure of **3**, there are three types of coordination modes for the H**SA/AS** ligand as in **1**: a μ_2-μ^1:μ^1 double monodentate bridging mode (scheme 1A), a μ_1-μ^1:μ^1 bidentate chelating mode (scheme 1B) and a μ_2-μ^1:μ^2 bridging mode (scheme 1C). Adjacent Sm ions are linked via μ_2-bridging carboxylate groups of the H**SA/AS** ligands to generate a binuclear building unit. The binuclear units are further connected through

C–H···π supramolecular interactions (table S5) to form a 2D network structure along the *ab* plane (figure 2b), extending to a 3D supramolecular structure (figure 2c).

In comparison, the lanthanides in **1** and **2** are eight-coordinate, in which Ho1 and Ho2 have a distorted bicapped trigonal prism geometry, while Ho3 is a distorted triangular dodecahedron, but nine-coordinate in **3**, in which the Sm1 has a distorted tricapped trigonal prism geometry, while Sm2 has a distorted monocapped square antiprism geometry. Complexes **1**-**3** contain the same coordination mode of the H**SA/SA** ligand. In **1** and **2**, the μ_2-bridging carboxylate groups of H**SA/SA** ligands linked the adjacent Ho ions to generate a trinuclear building unit. With respect to **3**, adjacent Sm centers are linked to form a binuclear building unit. Comparison of the structural differences between **1/2** and **3** suggests that the identity of metal plays an important role in the construction of such complexes. The structures all contain numerous weak interactions, C–H···O hydrogen bonding interactions or/and C–H···π supramolecular interactions which further connect the trinuclear units of **1** and **2** as well as binuclear units of **3** to lead to the final 3D supramolecular networks.

3.2. *XRPD Results*

To confirm whether the crystal structures are truly representative of the bulk materials, X-ray powder diffraction (XRPD) experiments were carried out. The XRPD experimental and computer-simulated patterns of the corresponding complexes are shown in figure S6 in the Supporting Information. The bulk synthesized materials and the as-grown crystals are homogeneous for **1**-**3**.

3.3. *Thermogravimetric analysis*

To examine the thermal stabilities of **1**-**3**, thermal gravimetric analysis (TGA) experiments were performed (see figure S7). **1** is stable to *ca*. 200 °C. After that, the weight loss is sharp, indicating decomposition of organic ligands and collapse of the framework. Similar thermogravimetric traces with decomposition temperatures of 200-600 °C are observed for **2**, suggesting that this complex possesses the same components and structure as **1** except for the different central lanthanide. With respect to **3**, it is thermally stable to *ca*. 220 °C. Upon further heating, pyrolysis of the organic ligands occurs, which does not stop before the heating ends at 900 °C.

3.4. *Magnetic properties*

Magnetic susceptibility data for a crushed crystalline sample of **1** were collected at an applied field of 0.3 T from 2–300 K. The data are shown in figure 3a as a χT vs. T plot (white circles). The χT product has a value of 43 cm^3 K mol^{-1} at 300 K, in agreement with the expected value for three isolated Ho(III) ions ($^5I_8$, S = 2, L = 6, J = 8 and g_J = 10/8). As temperature decreases, so does the χT product, until below 50 K a sharp decrease to a χT value of 23 cm^3 K mol^{-1} is observed, indicating depopulation of the excited Stark sublevels. Magnetization vs. field data for **1** are shown in figure 3b as a $M/N\mu_B$ vs. field plot. The curves are typical of lanthanide ions with strong spin-orbit coupling, as expected for Ho(III) complexes. The data eventually reach 16.1 μ_B at 1.8 K and 5 T. This value is lower than the expected saturation value for three Ho(III) ions, likely due to anisotropy and important crystal-field effects [14] at the Ln^{III} ion that eliminate the degeneracy of the ground state [15].

3.5. *Luminescent properties*

The luminescence spectra of **2** and **3** were investigated in the solid-state at room temperature and exhibit clear emission spectra of the corresponding Er^{III} and Sm^{III} ions as shown in figure 4. For **2**, the photoluminescent spectrum of Er^{III} in the near-infrared region was tested using excitation vis UV radiation. The Er^{III} complex displays an emission band at 1540 nm under excitation at 340 nm (figure 4a), and should be attributed to the transition of $^4I_{13/2} \rightarrow {}^4I_{15/2}$ [16]. In the case of **3**, under excitation at 340 nm, the spectrum exhibits four emission peaks at 565, 599, 646 and 701 nm (assignable to the $^4G_{5/2} \rightarrow {}^6H_J$ (J = 5/2, 7/2, 9/2, 11/2) transitions), characteristic of Sm^{III} and consistent with literature reports (figure 4b) [5b, 17].

4. Conclusion

We synthesized three lanthanide complexes incorporating mixed salicylate and phen ligands, $Ln_3(\mathbf{HSA})_5(\mathbf{SA})_2(phen)_3$ [Ln = Ho (**1**) and Er (**2**)] and $Sm_2(\mathbf{HSA})_2(\mathbf{SA})_2(phen)_3$ (**3**). Complexes **1** and **2** are isostructural with a trinuclear pattern, whereas **3** displays a binuclear structure. Comparison of the structural differences between **1/2** and **3** suggests that the identity of the metal plays an important role in such complexes. The magnetic properties of **1** were investigated and it exhibits the typical character of Ho ion. The Sm^{III} complex shows luminescence in the visible

region at excitation and the Er^{III} complex displays its characteristic luminescence in the near-infrared region. Further work on the H_2**SA**-based coordination polymers with other rare-earth ions is underway in our laboratory for developing more interesting functional coordination polymers.

Acknowledgements

This work was supported by the National Natural Science Foundation of China (21471134), Plan for Scientific Innovation Talent of Henan Province (154200510011) and Program for Science & Technology Innovative Research Team in University of Henan Province (No. 15IRTSTHN-002).

References

[1] (a) A.Y. Robin, K.M. Fromm. *Coord. Chem. Rev.*, **250**, 2127 (2006). (b) N. Wei, M.-Y. Zhang, X.-N. Zhang, G.-M. Li, X.-D. Zhang, Z.-B. Han. *Cryst. Growth Des.*, **14**, 3002 (2014). (c) Z.-N. Wang, X.-T. Xu, X. Lv, F.-Y. Bai, S.-Q. Liu, Y.-H. Xing. *RSC Adv.*, **5**, 104263 (2015). (d) A.J. Calahorro, I. Oyarzabal, B. Fernández, J.M. Seco, T. Tian, D. Fairen-Jimenez, E. Colacio, A. Rodríguez-Diéguez. *Dalton Trans.*, **45**, 591 (2016). (e) J.-C.G. Bünzli. *J. Coord. Chem.*, **67**, 3706 (2014).

[2] (a) Y. Cui, Y. Yue, G. Qian, B. Chen. *Chem. Rev.*, **112**, 1126 (2012). (b) Y. Han, X. Li, L. Li, C. Ma, Z. Shen, Y. Song, X. You. *Inorg. Chem.*, **49**, 10781 (2010). (c) Z. Ahmed, K. Iftikhar. *Inorg. Chem.*, **54**, 11209 (2015). (d) X. Lian, D. Zhao, Y. Cui, Y. Yang, G. Qian. *Chem. Commun.*, **51**, 17676 (2015). (e) H.-Y. Li, Y.-L. Wei, X.-Y. Dong, S.-Q. Zang, T.C.W. Mak. *Chem. Mater.*, **27**, 1327 (2015).

[3] (a) D.N. Woodruff, R.E.P. Winpenny, R.A. Layfield. *Chem. Rev.*, **113**, 5110 (2013). (b) K. Liu, H. Li, X. Zhang, W. Shi, P. Cheng. *Inorg. Chem.*, **54**, 10224 (2015). (c) M. Du, M. Chen, X. Wang, J. Wen, X.-G. Yang, S.-M. Fang, C.-S. Liu. *Inorg. Chem.*, **53**, 7074 (2014). (d) J.J. Baldov, E. Coronado, A. Gaita-Ariño, C. Gamer, M. Giménez-Marqués, G. Mínguez-Espallargas. *Chem.–Eur. J.*, **20**, 10695 (2014).

[4] (a) M. Du, C.-P. Li, C.-S. Liu, S.-M. Fang. *Coord. Chem. Rev.*, **257**, 1282 (2013). (b) B. Xu, Q. Chen, H.-M. Hu, R. An, X. Wang, G. Xue. *Cryst. Growth Des.*, **15**, 2318 (2015). (c) L. Zhang, C.-Y. Jing, Y.-Q. Zhong, Q.-H. Meng, K.-L. Zhang. *J. Coord. Chem.*, **68**, 3954 (2015). (d) X.T. Rao, T. Song, J.K. Gao, Y.J. Cui, Y. Yang, C.D. Wu, B.L. Chen,

G.D. Qian. *J. Am. Chem. Soc*., **135**, 15559 (2013). (e) Y.J. Cui, Y.F. Yue, G.D. Qian, B.L. Chen. *Chem. Rev*., **112**, 1126 (2012). (f) C. Chen, J. Zhang, Y. Zhang, Z. Yang, H. Wu, G. Pan, Y. Bai. *J. Coord. Chem*., **68**, 1054 (2015). (g) B.Cristóvão, J. Kłak, B. Miroslaw. *J. Coord. Chem*., **67**, 2728 (2014).

[5] (a) A. Louie. *Chem. Rev*., **110**, 3146 (2010). (b) M.D. Allendorf, C.A. Bauer, R.K. Bhakta, R.J.T. Houk. *Chem. Soc. Rev*., **38**, 1330 (2009). (c) Y.-H. Luo, F.-X. Yue, X.-Y. Yu, X. Chen, H. Zhang. *CrystEngComm*, **15**, 6340 (2013). (d) C. Yang, L.-M. Fu, Y. Wang, J.-P. Zhang, W.-T. Wong, X.-C. Ai, Y.-F. Qiao, B.-S. Zou, L.-L. Gui. *Angew. Chem., Int. Ed*., **43**, 5010 (2004). (e) P.P. Lima, M.M. Nolasco, F.A.A. Paz, R.A.S. Ferreira, R.L. Longo, O.L. Malta, L.D. Carlos. *Chem. Mater.*, **25**, 586 (2013).

[6] (a) X.-J. Zhang, Y.-H. Xing, Z. Sun, J. Han, Y.-H. Zhang, M.-F. Ge, S.-Y. Niu. *Cryst. Growth Des*., **7**, 2041 (2007). (b) B. Cai, Y. Ren, H. Jiang, D. Zheng, D. Shi, Y. Qian, H. Hu. *Inorg. Chem. Commun*., **15**, 159 (2012). (c) M. Chen, C. Wang, M. Hu, C.-S. Liu. *Inorg. Chem. Commun*., **17**, 104 (2012). (d) M. Dan, A.K. Cheetham, C.N.R. Rao. *Inorg. Chem*., **45**, 8227 (2006). (e) H. Xu, Y. Li. *J. Mol. Struct*., **690**, 137 (2004).

[7] (a) N. Zhao, S.-P. Wang, R.-X. Ma, Z.-H. Gao, R.-F. Wang, J.-J. Zhang. *J. Alloys Compd*., **463**, 338 (2008). (b) M.-C. Yin, C.-C. Ai, L.-J. Yuan, C.-W. Wang, J.-T. Sun. *J. Mol. Struct*., **691**, 33 (2004). (c) M.-C. Yin, L.-J. Yuan, C.-C. Ai, C.-W. Wang, E-T. Yuan, J.-T. Sun. *Polyhedron*, **23**, 529 (2004). (d) C.-S. Liu, M. Du, E.C. Sãnudo, J. Echeverria, M. Hu, Q. Zhang, L.-M. Zhou, S.-M. Fang. *Dalton Trans*., **40**, 9366 (2011). (e) D. Hu, F. Luo, J. Zheng. *J. Coord. Chem*., **60**, 1157 (2007).

[8] (a) R. Murugavel, R. Korah. *Inorg. Chem*., **46**, 11048 (2007). (b) C.-S. Liu, E.C. Sãnudo, M. Hu, L.-M. Zhou, L.-Q. Guo, S.-T. Ma, L.-J. Gao, S.-M. Fang. *CrystEngComm*, 2010, **12**, 853 (2010).

[9] *SAINT Software Reference Manual*; Bruker AXS: Madison, WI (1998).

[10] G.M. Sheldrick and *SADABS*, *Siemens Area Detector Absorption Corrected Software*, University of Göttingen: Göttingen, Germany (1996).

[11] (a) G.M. Sheldrick, *SHELXTL NT Version 5.1. Program for Solution and Refinement of Crystal Structures*, University of Göttingen: Göttingen, Germany (1997). (b) G.M. Sheldrick. *Acta Cryst*., A**64**, 112 (2008).

[12] (a) H.-N. Li, H.-Y. Li, L.-K. Li, L. Xu, K. Hou, S.-Q. Zang, T.C.W. Mak. *Cryst. Growth Des*., **15**, 4331 (2015). (b) K.-L. Hou, F.-Y. Bai, Y.-H. Xing, J.-L. Wang, Z. Shi. *CrystEngComm*, **13**, 3884 (2011). (c) X.-J. Zheng, Z.-M. Wang, S. Gao, F.-H. Liao, C.-H. Yan, L.-P. Jin. *Eur. J. Inorg. Chem*., 2968 (2004). (d) Y.-Y. Zhang, N. Ren, S.-L. Xu, J.-J. Zhang, D.-H. Zhang. *J. Mol. Struct*., **1081**, 413 (2015).

[13] (a) Y.-S. Song, B. Yan. *Inorg. Chim. Acta*, **358**, 191 (2005). (b) S. Su, W. Chen, C. Qin, S. Song, Z. Guo, G. Li, X. Song, M. Zhu, S. Wang, Z. Hao, H. Zhang. *Cryst. Growth Des*., **12**, 1808 (2012). (c) J.-C. Zhong, F. Wan, Y.-Q. Sun, Y.-P. Chen. *J. Solid State Chem*., **221**, 14 (2015).

[14] M.A. AlDamen, J.M. Clemente-Juan, E. Coronado, C. Martí-Gastaldo, A. Gaita-Arinño. *J. Am. Chem. Soc*., **130**, 8874 (2008).

[15] S. Osa, T. Kido, N. Matsumoto, N. Re, A. Pochaba, J. Mrozinski. *J. Am. Chem. Soc*., **126**, 420 (2004).

[16] (a) M. Hu, H. Zhao, E.C. Sañudo, M. Chen. *Polyhedron*, **101**, 270 (2015). (b) H.-S. Wang, B. Zhao, B. Zhai, W. Shi, P. Cheng, D.-Z. Liao, S.-P. Yan. *Cryst. Growth Des*., **12**, 2602 (2012). (c) B. Li, W. Gu, L.Z. Zhang, J. Qu, Z.P. Ma, X. Liu, D.Z. Liao. *Inorg. Chem*., **45**, 10425 (2006).

[17] (a) X.-L. Li, C.-L. Chen, H.-P. Xiao, A.-L. Wang, C.-M. Liu, X. Zheng, L.-J. Gao, X.-G. Yang, S.-M. Fang. *Dalton Trans*., **42**, 15317 (2013). (b) F. Zhang, X.-T. Huang, Y.-Y. Tian, Y.-X. Gong, X.-Y. Chen, J.-J. Lin, D.-S. Lu, Y.-L. Zhang, R.-H. Zeng, S.-R. Zheng. *J. Coord. Chem*., **66**, 2659 (2013). (c) D.-P. Dong, L. Liu, Z.-G. Sun, C.-Q. Jiao, Z.-M. Liu, C. Li, Y.-Y. Zhu, K. Chen, C.-L. Wang. *Cryst. Growth Des*., **11**, 5346 (2011).

Table 1. Crystallographic data and structure refinement summary for **1**-**3**.[a]

	1	**2**	**3**
Chemical formula	$C_{85}H_{57}Ho_3N_6O_{21}$	$C_{85}H_{57}Er_3N_6O_{21}$	$C_{64}H_{42}N_6O_{12}Sm_2$
Formula mass	1993.16	2000.15	1387.74
Crystal system	Monoclinic	Monoclinic	Monoclinic
Space group	*P*2(1)/*c*	*P*2(1)/*c*	*P*2(1)/*c*
a/Å	14.2446(2)	14.2353(3)	10.9077(4)
b/Å	23.2892(4)	23.2985(5)	28.5413(11)
c/Å	23.7871(4)	23.7963(6)	18.3989(5)
β/°	103.462(2)	103.481(2)	104.110
V/Å^3	7674.4(2)	7674.9(3)	5555.1(3)
T/K	294(2)	294(2)	294(2)
Z	4	4	4
μ/mm^{-1}	3.144	3.331	2.165
R_{int}	0. 0245	0.0277	0.0509
[a]R_1 ($I > 2\sigma(I)$)	0.0247	0.0239	0.0450
[b]wR_2 (all data)	0.0548	0.0447	0.1126
GOF	0.925	0.827	1.034

[a] $R_1 = \Sigma(||F_o| - |F_c||)/\Sigma|F_o|$; [b] $wR_2 = [\Sigma w(|F_o|^2 - |F_c|^2)^2/\Sigma w(F_o^2)^2]^{1/2}$.

Figure captions

Figure 1. Views of **1**: (a) the unit structure, (b) the 1D chain and (c) the 3D supramolecular structure via C–H···O hydrogen bonds (blue dashed lines) and C–H···π supramolecular interactions (black dashed lines).

Figure 2. Views of **3**: (a) the unit structure, (b) the 2D network and (c) the 3D supramolecular structure via C–H···π supramolecular interactions (black dashed lines).

Figure 3. (a) χT vs. T plot for **1** at an applied dc field of 3 T from 300 to 2 K; (b) reduced magnetization plot for **1** at 2 K.

Figure 4. Solid-state emission spectra of (a) **2** and (b) **3**.

Figure 1.

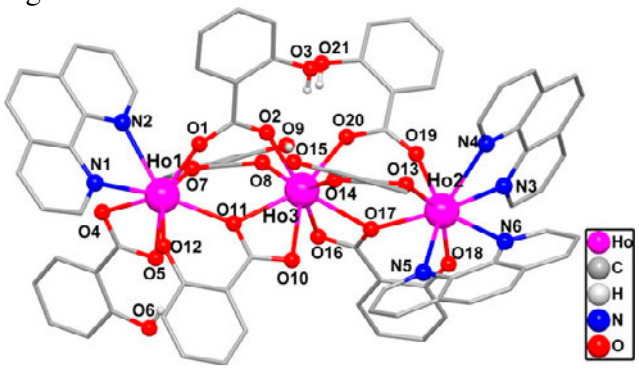

(a)

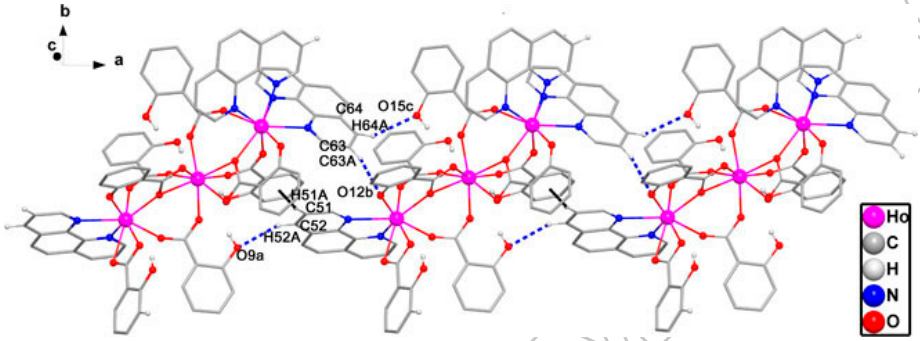

(b)

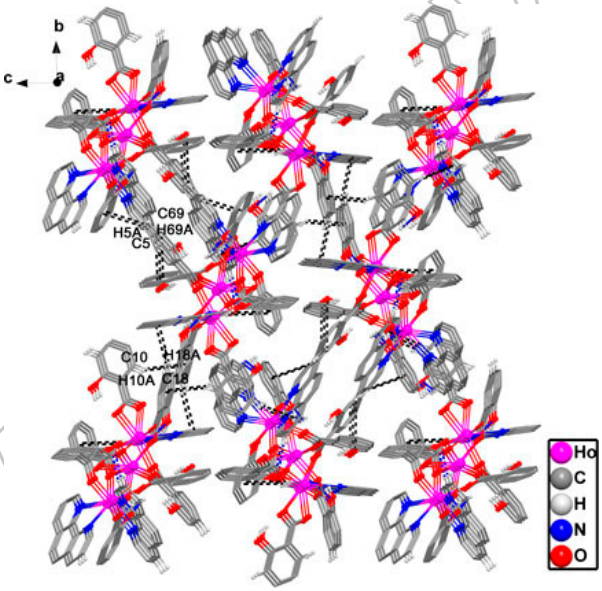

(c)

Figure 2.

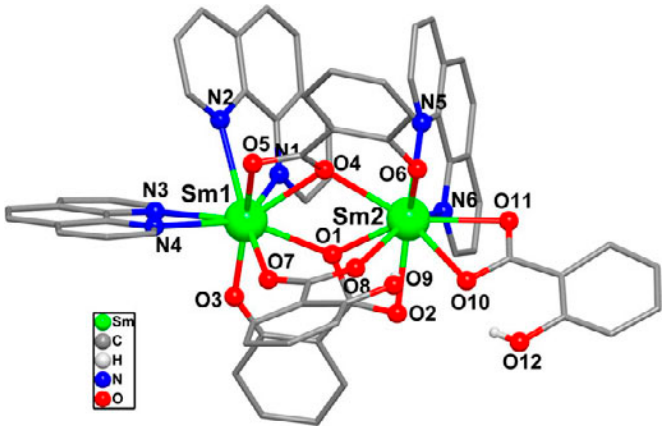

(a)

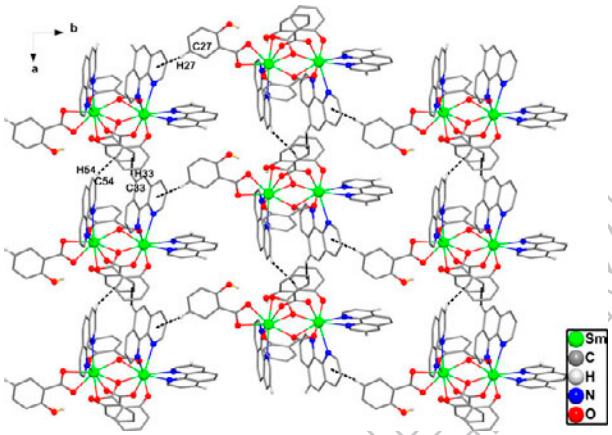

(b)

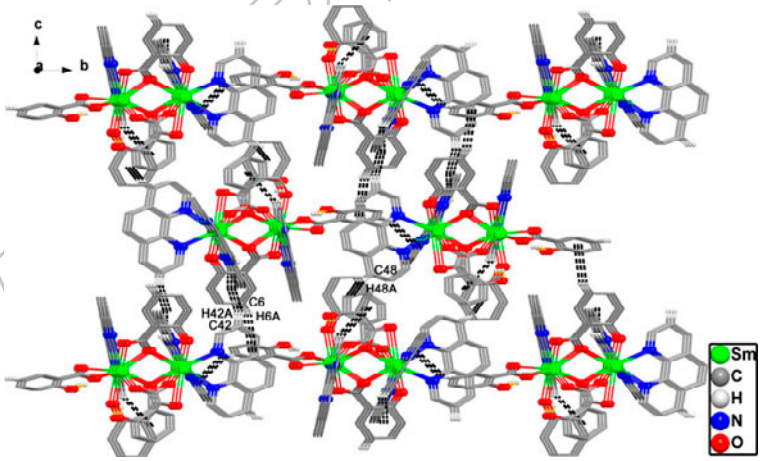

(c)

Figure 3.

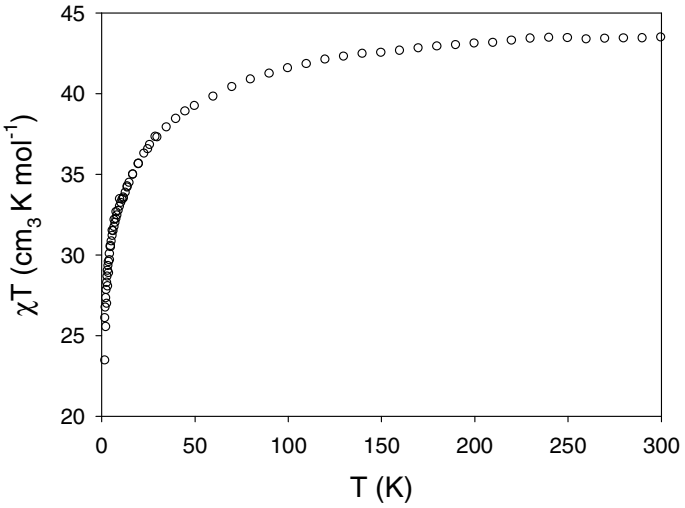

(a)

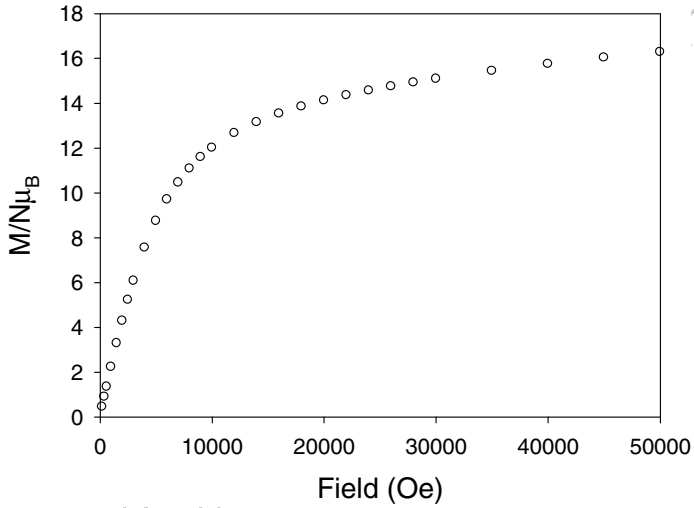

(b)

Figure 4.

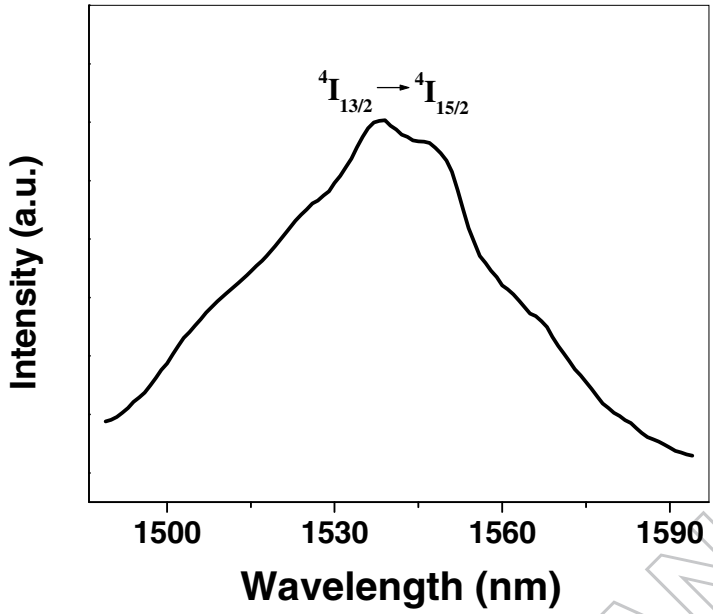

(a)

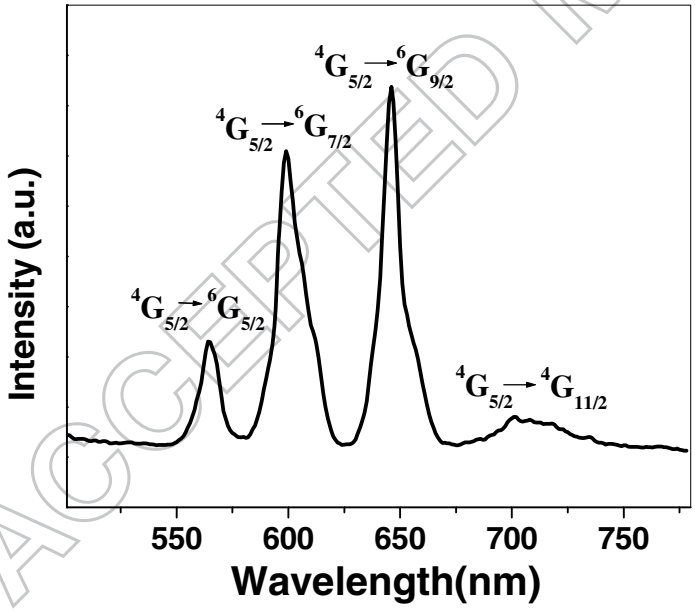

(b)

Graphical abstract